

CO Clouds around SNR G21.8–0.6 and G32.8–0.1 *

Jian-Jun Zhou^{1,2,3}, Xi-Zhen Zhang¹, Hong-Bo Zhang¹, Jarken Esimbek², Ju-Yong Zhang¹ and Bing-Gang Ju⁴

¹ National Astronomical Observatories, Chinese Academy of Sciences, Beijing 100012;
zhoujj@ms.xjb.ac.cn

² National Astronomical Observatories / Urumqi Observatory, Chinese Academy of Sciences, Urumqi 830011

³ Graduate School of Chinese Academy of Sciences, Beijing 100049

⁴ Qinghai Station of Purple Mountain Observatory, Chinese Academy of Sciences, Delingha 817000

Received 2006 December 14; accepted 2007 April 5

Abstract We made the first CO(1–0) mapping to SNR G21.8–0.6 and SNR G32.8–0.1, both associated with OH 1720 MHz maser. Based on the morphological correspondence and velocity and position agreement between the radio remnant and the CO clouds, we tentatively identify the clouds that are respectively interacting with the two SNRs.

Key words: ISM: clouds — ISM: individual (G21.8–0.6, G32.8–0.1) — ISM: molecules — masers — supernova remnants

1 INTRODUCTION

Massive stars usually do not drift far from their parent clouds before they finish their life as supernova, when the shock driven into the clouds will accelerate relativistic particles, heat and compress the molecular gas, and change its chemistry. The turbulence caused by the shock may trigger the formation of a new generation of stars. Therefore, the interaction between Supernova Remnants (SNRs) and molecular clouds plays a very important role in the evolution of star and Interstellar Medium (ISM) (Frail et al. 1994; Reynoso et al. 2000). The study of such interactions will help us to understand the involved processes. However, it is not easy to determine unambiguously whether or not an SNR is physically associated with a molecular cloud, e.g., they may appear as positionally coincident just because of confusion introduced by unrelated gas along the line of sight. Many criteria have been used to do this, which include: (1) Morphological signatures, such as arcs of gas outlining an SNR or indentations in SNR edges surrounding gas concentrations (Landecker et al. 1989; Reynoso et al. 1995; Duber et al. 1999); (2) Radio continuum enhancement (Reynoso et al. 2000); (3) Spectral line broadenings (Frail & Mitchell 1998; Reach & Rho 1999) or spectral wings (Seta et al. 1998); (4) IR emission from shock-heated dust (Reynoso et al. 2000).

Recently, OH 1720 MHz masers have been identified as one sure signature of SNR-molecular cloud interaction (Frail et al. 1994; Yusef-Zadeh et al. 2003). The excitation of OH 1720 MHz maser requires a very dense gas ($\sim 10^5 \text{ cm}^{-3}$) with a temperature of 50–125 K. A C-type shock caused by the expanding supernova remnant will create such conditions (Elitzur 1976; Wardle 1999; Lockett et al. 1999). This has been proven to be true by many molecular line observations to SNRs associated with OH 1720 MHz masers (Koralesky et al. 1998; Reach & Rho 1998; Frail & Mitchell 1998; Reynoso et al. 2000).

We carried out the CO(1–0) observations to the SNR G21.8–0.6 and G32.8–0.1, which are associated with 1720 MHz OH masers. We hope to study the relation between the SNRs and ambient CO clouds and search for the effects of SNR-molecular cloud interaction. These observations will provide the basis for future study through higher transitions.

* Supported by the National Natural Science Foundation of China.

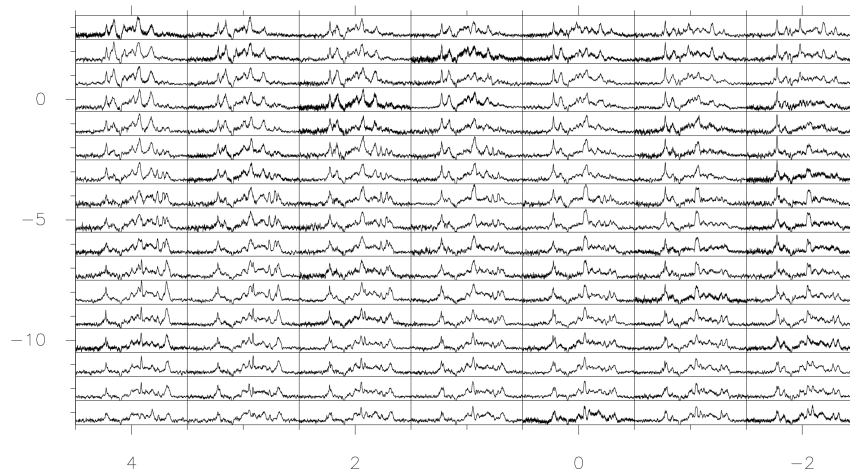


Fig. 1 Mosaic of $^{12}\text{CO}(1-0)$ spectra in SNR G21.8–0.6. Here (0,0) refers to the position of OH maser (R.A. = $18^{\text{h}}33^{\text{m}}11.97^{\text{s}}$, DEC = $-10^{\circ}00'40.16''$) (J2000). The velocity scale in each spectrum runs from $V_{\text{LSR}} = -50$ to $+160 \text{ km s}^{-1}$ and the antenna temperature scale from $T_{\text{A}} = -1$ to $+5 \text{ K}$.

2 OBSERVATIONS

Observations of the $^{12}\text{CO}(1-0)$ line and its isotopes were carried out with the 13.7 m telescope located at Delingha, Qinghai province of China, in April 2004. The half-power beam size of the telescope at the frequency 112 GHz is about $106'' \times 70''$, the pointing accuracy is better than $10''$ (rms). We observed $\text{CO}(1-0)$ and its two isotopes simultaneously. The frequency resolutions at $^{12}\text{CO}(1-0)$, $^{13}\text{CO}(1-0)$ and $\text{C}^{18}\text{O}(1-0)$ are 209 kHz, 78.7 kHz and 75.7 kHz, respectively. The sensitivity of the telescope is 0.26 K (rms) for an integration time of 60 second. The position-switching mode was used. Both maps cover an area of $35' \times 35'$, at steps of $60''$ in both Right Ascension and Declination.

3 RESULTS

Here we give a brief description of these remnants and the results of our $\text{CO}(1-0)$ observation. There is a dip in the spectra of G21.8–0.6 between 30 and 40 km s^{-1} (see Figs. 1 and 2), which seems to be evidence of self-absorption. However, a careful examination of the off-spectra indicates that there is emission at the same velocity range at the off-position. Because G21.8–0.6 is close to the Galactic plane, it is difficult to find a very clear off-position, but the small dip appearing in the spectra of G32.8–0.1 between 0 and 10 km s^{-1} (Figs. 4 and 5) may be caused by self-absorption. If this is true, self-observation would be weak. The $^{13}\text{CO}(1-0)$ emissions of these two SNRs are very weak, while $\text{C}^{18}\text{O}(1-0)$ was not detected at all at rms 0.26 K.

3.1 G21.8–0.6

G21.8–0.6 is an SNR with an incomplete radio shell morphology (Fig. 3), the continuum image was obtained from the radio continuum survey of the Galactic plane at 11 cm wavelength (Reich et al. 1984). The HII region G21.9–0.4, located to the northwest of the SNR, is unrelated to the SNR (Fig. 3). The OH 1720 MHz maser associated with the SNR is marked with a plus sign in Figure 3. It has a velocity of 69.3 km s^{-1} (Frail & Mitchell 1998; Green et al. 1997). G21.8–0.6 has a systemic velocity of 82 km s^{-1} , corresponding to a kinematic distance of 11.2 kpc, so the linear size of G21.8–0.6 is about 80 pc (Kassim 1992; Green 1997). The brightest X-ray feature lies in the interior of the radio shell of the SNR and form two halves of a shell-like structure (Yusef-Zadeh et al. 2003).

The CO line profiles observed in G21.8–0.6 are complex (Fig. 1). The mosaic of $^{12}\text{CO}(1-0)$ spectra covers the bright eastern rim of G21.8–0.6 (Fig. 3), they show rapidly varying profiles across the mapping

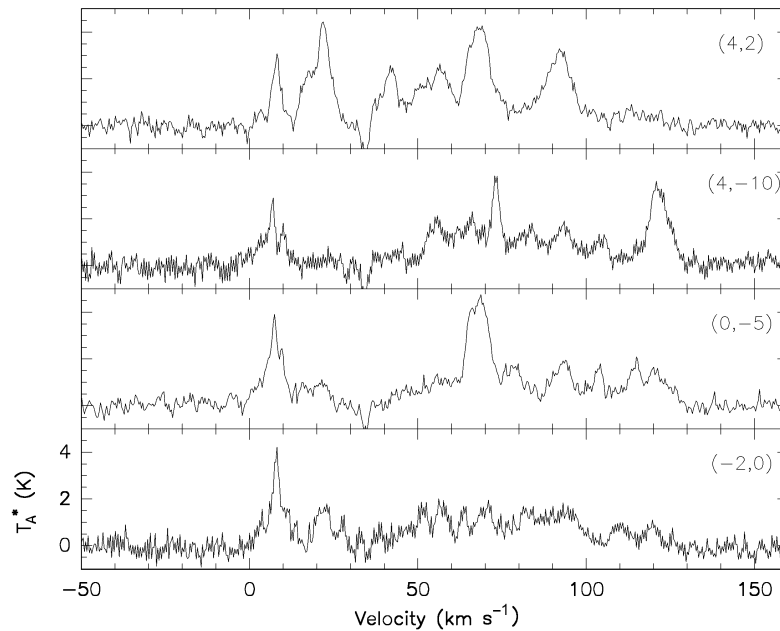


Fig. 2 Blow-up of ^{12}CO (1–0) spectra at selected positions in SNR G21.8–0.6. Offsets in arcmin from (0,0) (R.A. = $18^{\text{h}}33^{\text{m}}11.97^{\text{s}}$, DEC = $-10^{\circ}00'40.16''$) (J2000) are indicated in the upper right corner. The integration time is 1 minute.

region. At least four different components with $\Delta V \approx 10 \text{ km s}^{-1}$ can be distinguished at $V_{\text{LSR}} \approx 21, 69, 92$ and 122 km s^{-1} . Figure 2 shows blow-ups of the profile at some positions, the offsets in arcmin from (0,0) (R.A. = $18^{\text{h}}33^{\text{m}}11.97^{\text{s}}$, DEC = $-10^{\circ}00'40.16''$) (J2000) are indicated in the upper right corner. The CO maps integrated over the four velocity ranges, 116–128, 86–98, 63–75 and 14–30 km s^{-1} are superimposed on the continuum map of the SNR in grey scale (see Fig. 3), and are labelled A, B, C and D. Cloud A appears to touch the bright south-western shell of the SNR, and more diffuse CO emission appears on the other side of the remnant. Cloud B overlaps with the north-eastern part of the remnant, the diffuse clouds in the map seems to consist of a ring like structure. The elongated cloud C overlaps with the bright continuum shell and covers more than half of the remnant. Cloud D shows an incomplete ring-like structure with a break in its south-eastern edge: it is where the SNR lies. The ring overlaps with the northern part of the remnant.

3.2 G32.8–0.1

G32.8–0.1 is an elongated shell-type SNR, scales approximately $20'$ (north-south) $\times 10'$ (east-west) (Kassim 1992; Clark et al. 1975). The VLA observation indicates that it has an incomplete ring-like structure, and the OH 1720 MHz maser with a velocity, $V_{\text{LSR}} = 86.1 \text{ km s}^{-1}$, is just located at the eastern edge of the ring (Koralesky et al. 1998). On the assumption that the shock is transverse to the line of sight, the LSR velocity of the SNR was found to be also 86.1 km s^{-1} (Frail et al. 1996; Claussen et al. 1997), which corresponds to either a near kinematic distance of 5.5 kpc or a far of that 8.8 kpc (Koralesky et al. 1998). Taking into consideration the results of Helfand et al. (1989), we think 8.8 kpc is the more reasonable value.

The CO(1–0) spectra of G32.8–0.1 are relatively simple, with a few blending features. A mosaic of the ^{12}CO (1–0) spectra along the eastern boundary of the remnant is displayed in Figure 4. Four components at $V_{\text{LSR}} \approx 18, 52, 78$ and 98 km s^{-1} show significantly varying profiles, and only the one component at 52 km s^{-1} has a line width $\Delta V \geq 10 \text{ km s}^{-1}$. Figure 5 shows blow-ups of the profile at some positions, the offsets in arcmin from (0,0) (R.A. = $18^{\text{h}}51^{\text{m}}23.97^{\text{s}}$, DEC = $-00^{\circ}08'22.54''$) (J2000) are indicated in the upper right corner.

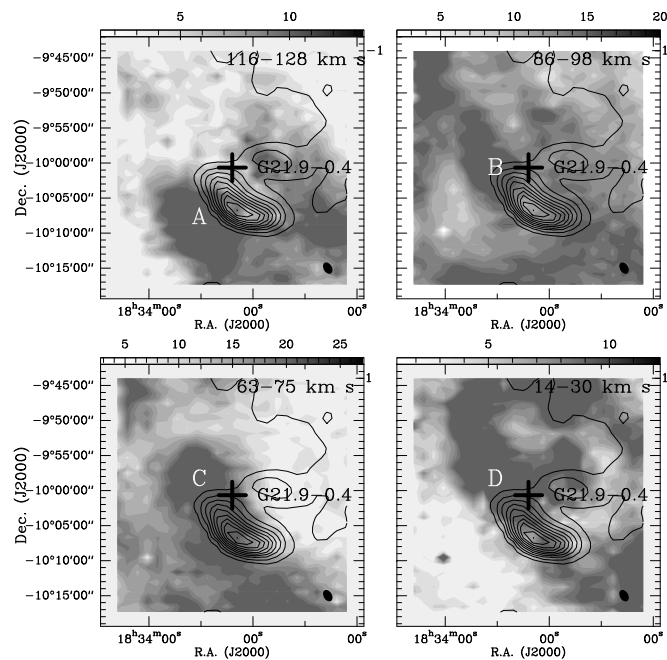


Fig. 3 Channel maps of $^{12}\text{CO}(1-0)$ emission toward G21.8–0.6 integrated over four velocity ranges, 116–128, 86–98, 63–75 and 14–30 km s^{-1} . The grey scale is in K km s^{-1} and is shown on top of the image. The 2σ noise level of these maps are 1.25, 1.65, 2.18 and 1.29 K km s^{-1} , respectively. The beam width, $106'' \times 70''$, is indicated by the filled ellipse in the bottom right corner. The contour map was obtained from the radio continuum survey of the Galactic plane at 11 cm wavelength (Reich et al. 1984), the contour levels are from 3.74 to 37.4 Jy in steps of 3.74 Jy. G21.9–0.4 is an HII region. The plus sign shows the position of the OH 1720 MHz maser.

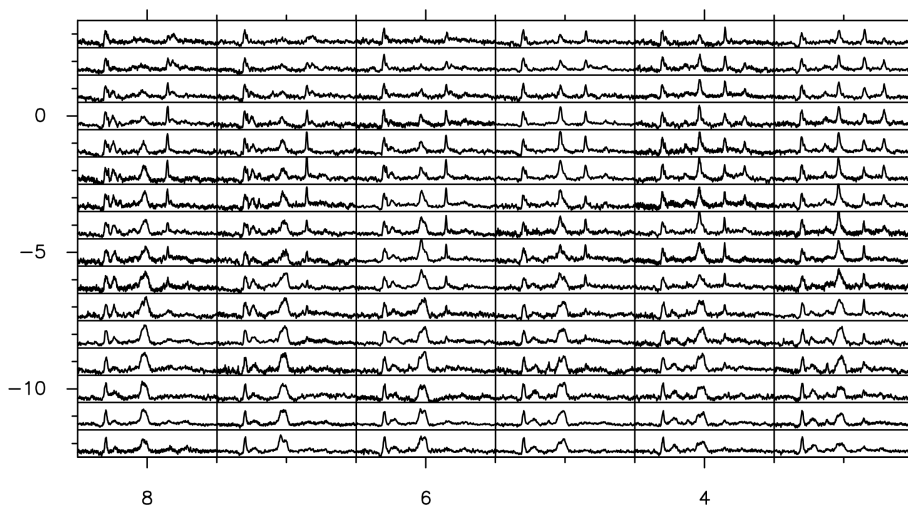


Fig. 4 Mosaic of $^{12}\text{CO}(1-0)$ spectra in SNR G32.8–0.1, it covers the eastern boundary of the remnant and the OH maser site. Here (0,0) refers to the position (R.A. = $18^{\text{h}}51^{\text{m}}23.97^{\text{s}}$, DEC = $-00^{\circ}08'22.54''$) (J2000). The velocity scale in each spectrum runs from $V_{\text{LSR}} = -20$ to $+130 \text{ km s}^{-1}$ and the antenna temperature scale from $T_{\text{A}} = -1$ to $+4 \text{ K}$.

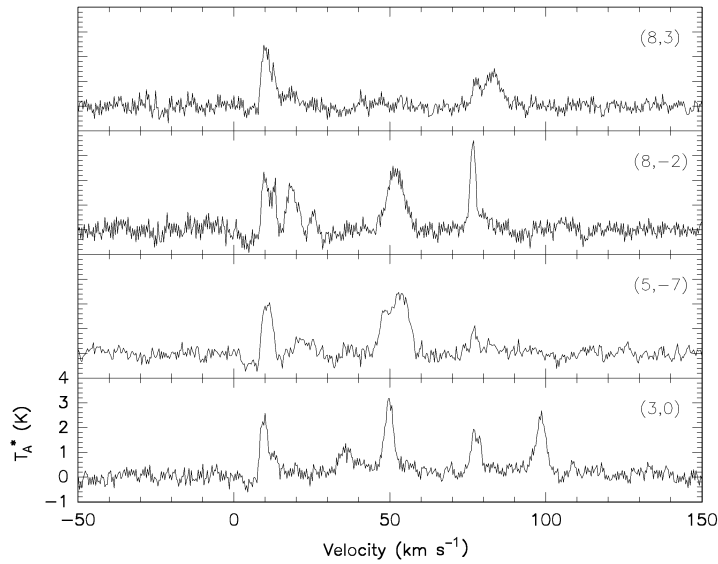


Fig. 5 Blow-up of $^{12}\text{CO}(1-0)$ spectra at selected positions in SNR G32.8–0.1. Offsets in arcminute from (0,0) (R.A. = $18^{\text{h}}51^{\text{m}}23.97^{\text{s}}$, DEC = $-00^{\circ}08'22.54''$) (J2000) are indicated in the upper right corner. The integration time is 1 minute.

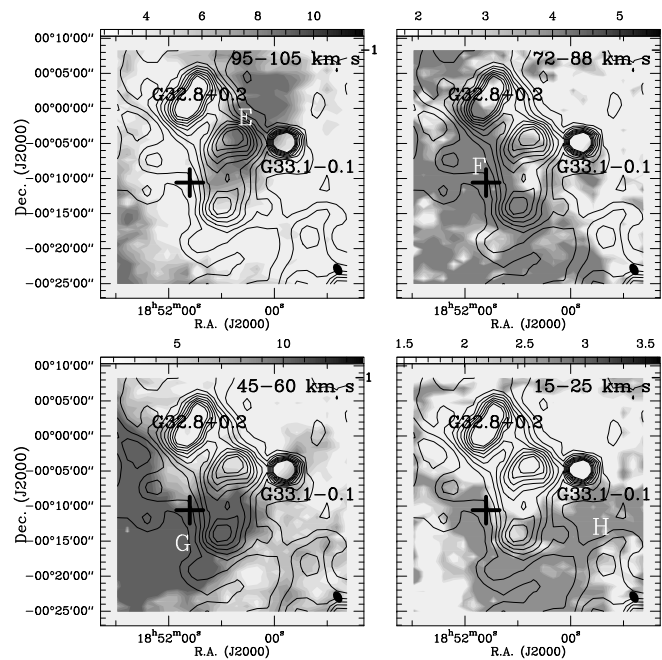


Fig. 6 Channel maps of $^{12}\text{CO}(1-0)$ emission integrated over the velocity ranges 95–105, 72–88, 45–60 and 15–25 km s^{-1} , respectively, toward G32.8–0.1. The grey scale is in K km s^{-1} and is shown on top of the images. The 2σ noise level of these maps are 1.46, 1.11, 1.53 and 0.99 K km s^{-1} , respectively. The beam width, $106'' \times 70''$, is indicated by the filled ellipse in the bottom right corner. The continuum contour of G32.8–0.1 was also obtained from the radio continuum survey of the Galactic plane at 11 cm wavelength (Reich et al. 1984), which includes two HII regions, G32.8+0.2 and G33.1–0.1 (Clark et al. 1975). The rms is about 50 mJy beam^{-1} . Contour levels are from 0.3 to 3 Jy in steps of 0.3 Jy. The plus sign indicates the position of the OH maser.

Channel maps of $^{12}\text{CO}(1-0)$ integrated over the velocity ranges 95–105, 72–88, 45–60 and 15–25 km s^{-1} are displayed in Figure 6, labelled E, F, G and H. Here the continuum contour of G32.8–0.1 was also taken from the radio continuum survey of the Galactic plane at 11 cm wavelength (Reich et al. 1984), which includes two HII regions, G32.8+0.2 and G33.1–0.1 (Clark et al. 1975)(see Fig. 6). One bright continuum peak appears on the northern shell of the SNR, and another weak one appears on the southern shell. The OH 1720 MHz maser was marked with a plus sign in these maps. Cloud E shows a long filamentary structure elongated nearly along the of northwest-southeast direction, it overlaps with the bright peak of the SNR, but it is not coincident with the OH maser. Cloud F is located to the east of the remnant, and overlaps with its eastern boundary. The edge of the radio continuum aligns perfectly with the edge of cloud F, and seems to form the interface where the SNR meets the ambient CO cloud. The OH maser coincides with this cloud. Cloud G is located to the east of the SNR, and its extension coincides with the weak continuum peak of the SNR. Cloud H is more diffuse, and overlaps with the southern part of the continuum shell. The OH maser lies in the boundary between Clouds G and H (see Fig. 6).

4 DISCUSSION

Shock-excited 1720 MHz OH masers toward SNRs constitute a powerful tool to ensure securely that the molecular structures at the same velocity of the masers are physically related to the remnants (Reynoso et al. 2000). The use of OH 1720 MHz masers as signposts of SNR-molecular cloud interaction allowed us to detect the molecular gas into which supernova shock fronts are being driven. In the following we will discuss the relation between the CO clouds and G21.8–0.6 and G32.8–0.1 in regard to their agreement in position and velocity, the morphological signature of the CO clouds and the spectral line broadenings.

G21.8–0.6 Because the passage of a C-type shock creates conditions needed for the excitation of OH 1720 MHz masers, the maximum amplification occurs along the edge of the SNR, where the least velocity dispersion and hence the largest coherence is maintained. The velocity of an OH 1720 MHz maser associated with an SNR can be identified with the systemic velocity of the remnant (Reynoso et al. 2000). Therefore the velocity agreement between the OH maser and CO clouds interacting with the SNR should be good. The OH 1720 MHz maser associated with G21.8–0.6 has an LSR velocity of 69.3 km s^{-1} , which is nearly the same as that of cloud C.

The excitation of OH 1720 MHz masers also indicates that the maser should have a good positional agreement with shock-excited molecular gas. The channel maps indicate that all the velocity components partly overlap with the continuum shell (Fig. 3). In the case of cloud A we can see close agreement between the steeply falling CO intensity and the steeply rising radio continuum intensity across the edge of the radio shell, while the OH 1720 MHz maser is far from this cloud. Cloud B overlaps with the northern part of G21.8–0.6, where the continuum shell shows no gross distortion which can be obviously linked to the SNR-molecular cloud interaction. This is also true for clouds C and D. Cloud C apparently wraps round the bright western continuum shell. The OH 1720 MHz maser is in the interior of clouds C and D.

For individual remnants associated with OH 1720 MHz maser, there exist morphological, kinematic and chemical signatures for molecular shocks. Spectral line broadenings are accepted as a very sure signature to determine whether shock excited molecular clouds exist (Reynoso et al. 2000), while the broadened spectral lines at the location of the masers have a width ($\Delta V \approx 10\text{--}50 \text{ km s}^{-1}$) (Koralesky et al. 1998). Here four components at $V_{\text{LSR}} \approx 21, 69, 92$ and 122 km s^{-1} all have line widths $\Delta V \approx 10 \text{ km s}^{-1}$ (Figs. 1 and 2), but the big velocity differences between the OH maser and CO clouds A, B and D indicate that they may not be shock excited. The complex spectra strongly suggest those velocity components may represent giant molecular clouds along the line of sight, where severe blending of velocity components may result in line broadening.

Taking into consideration the position and velocity agreement between the clouds and OH maser, and the morphology of the CO cloud, we tentatively suggest that cloud C is a possible candidate interacting with G21.8–0.6.

G32.8–0.1 For G32.8–0.1, the OH 1720 MHz maser is also the most convincing proof of SNR-molecular cloud interaction. It has a velocity of 86.1 km s^{-1} . The four velocity components are centered at $V_{\text{LSR}} \approx 18, 52, 78$ and 98 km s^{-1} , respectively, so the best velocity agreement was found between the OH maser and cloud F (Fig. 5), with a velocity difference of about 8 km s^{-1} . Such a velocity difference can be

well explained by the suggestion of Koralesky et al., that the OH maser originates in shocks transverse to the line of sight (Koralesky et al. 1998).

The distribution of these four components (Fig. 6) also partly overlap with the continuum shell. The map of cloud E shows no gross distortion that can be obviously linked to SNR-molecular cloud interaction, and the OH maser does not coincide with it. A striking agreement in position was found between the OH maser and cloud F, with the maser lying inside the cloud, and the edge of the radio continuum aligning perfectly with the edge of cloud F (Fig. 6). This cloud seems to be ramming the eastern continuum shell. The OH maser coincides with the edge of cloud G, and this cloud also shows some distortion that indicates interaction. Cloud H is a more diffuse cloud.

A mosaic of CO(1–0) spectra covers the eastern boundary of the continuum shell of G32.8–0.1, where the OH maser lies (Fig. 6). The four velocity components vary significantly in line width and intensity (Figs. 4 and 5), only the component at $V_{\text{LSR}} \approx 52 \text{ km s}^{-1}$ has a line width $\Delta V \geq 10 \text{ km s}^{-1}$, which seems to consist of at least two features blending into this relatively broad line width. The variation of these features in intensity may be the reason why this velocity component shows flattened peaks (Fig. 4). We did not find line broadenings at 78 km s^{-1} . A possible reason is that the shocked molecular gas may be highly excited and therefore weak in emission from the low-lying CO(1–0) transition (Wilner et al. 1998), and confusion caused by different clouds along the line of sight makes it difficult to detect such weak broad CO(1–0) emission. Similarly, we tentatively suggest that cloud F may be interacting with G32.8–0.1.

5 CONCLUSIONS

Based on the morphological signature of CO clouds and the position and velocity agreement between the OH maser and CO clouds, we tentatively suggest that cloud C of G21.8–0.6 and cloud F of G32.8–0.1 may be physically related to the SNR. However, we did not find any line broadenings in cloud F, and it is not obvious in cloud C. A possible reason is that the shocked molecular gas may be highly excited and therefore weak in emission from the low-lying CO(1–0) transition. Worse, the background cloud emission could mask such weak features. Taking into consideration the complexity of the CO(1–0) spectra, we think that confusion due to different velocity components along the line of sight plays an important role here, which makes discerning of line broadenings difficult.

Acknowledgements This Work was funded by the Program of the Light in China’s Western Region under the grant Nos RCPY200605 and ZZBS 200601, and partly by the National Natural Science Foundation of China through Grant 10203003.

References

- Clark D. H., Caswell J. L., Green A. J., 1975, *AuJPAS*, 37, 1
 Claussen M. J., Frail D. A., Goss W. M., Gaume R. A., 1997, *ApJ*, 489, 143
 Dubner G. M., Giacani E. B., Giacani E. M., Goss W. M., Roth M., Green A. J., 1999, *AJ*, 118, 930
 Elitzur M., 1976, *ApJ*, 203, 124
 Frail D. A., Goss W. A., Slysh V. I., 1994, *ApJ*, 424, L111
 Frail D. A., Goss W. M., Reynoso E. M., Giacani E. B., Goss W. M., Duber G., 1996, *AJ*, 111, 1651
 Frail D. A., Mitchell G. F., 1998, *ApJ*, 508, 690
 Green A. J., Frail D. A., Goss W. M., Otrupcek R., 1997, *AJ*, 114, 2058
 Helfand D. J., Vellusamy T., Becker R. H., Lockman F. J., 1989, *ApJ*, 341, 151
 Kassim N. E., 1992, *AJ*, 103, 943
 Koralesky B., Frail D. A., Goss W. M., Claussen M. J., Green A. J., 1998, *AJ*, 116, 1323
 Landecker T. L., Pineault S., Routledge D., Vaneldik J. F., 1989, *MNRAS*, 237, 277
 Lockett T. L., Gauthier E., Elitzur M., 1999, *ApJ*, 511, 235
 Reach W. T., Rho J., 1998, *ApJ*, 507, L93
 Reach W. T., Rho J., 1999, *ApJ*, 511, 836
 Reich W., Fürst E., Steffen P., Reif K., Haslam C. G., 1984, *A&AS*, 58, 197
 Reynoso E. M., Mangum J. G., 2000, *ApJ*, 545, 874
 Reynoso E. M., Dubner G. M., Goss W. M., Arnal E. M., 1995, *AJ*, 110, 318
 Seta M., Hasegawa T., Dame T. et al., 1998, *ApJ*, 505, 286
 Wardle M., 1999, *ApJ*, 525, L101
 Wilner D. J., Reynoso S. P., Moffett D. A., 1998, *ApJ*, 115, 247
 Yusef-Zadeh F., Wardle M., Rho J., Sakano M., 2003, *ApJ*, 585, 319